# Microchannel Thermal Management System With Two-Phase Flow for Power Electronics Over 500 W/cm 2 Heat Dissipation — Source link

Fengze Hou, Hengyun Zhang, Dezhu Huang, Jiajie Fan ...+6 more authors

Institutions: Chinese Academy of Sciences, Shanghai University of Engineering Sciences, Delft University of Technology, Lamar University ...+1 more institutions

Topics: Heat sink, Heat flux, Junction temperature, Microchannel and Condenser (heat transfer)

Related papers:

- Experimental Research on a Honeycomb Microchannel Cooling System

- A Honeycomb Microchannel Cooling System for Microelectronics Cooling

- High Heat Flux Two-Phase Cooling in Silicon Multimicrochannels

- Experimental evaluation of a compact two-phase cooling system for high heat flux electronic packages

- Flow Boiling of R134a in a Multi-Microchannel Heat Sink With Hotspot Heaters for Energy-Efficient Microelectronic CPU Cooling Applications

# Delft University of Technology

## Microchannel Thermal Management System with Two-Phase Flow for Power Electronics over 500 W/cm2Heat Dissipation

Hou, Fengze; Zhang, Hengyun; Huang, Dezhu; Fan, Jiajie; Liu, Fengman; Lin, Tingyu; Cao, Liqiang; Fan, Xuejun; Ferreira, Braham; Zhang, Guoqi

**Citation (APA)**
Hou, F., Zhang, H., Huang, D., Fan, J., Liu, F., Lin, T., Cao, L., Fan, X., Ferreira, B., & Zhang, G. (2020). Microchannel Thermal Management System with Two-Phase Flow for Power Electronics over 500 W/cm$^2$Heat Dissipation. *IEEE Transactions on Power Electronics*, *35*(10), 10592-10600. [9057466]. https://doi.org/10.1109/TPEL.2020.2985117

**Important note**
To cite this publication, please use the final published version (if applicable).
Please check the document version above.

# Microchannel Thermal Management System with Two-Phase Flow for Power Electronics over 500 W/cm² Heat Dissipation

Fengze Hou, Hengyun Zhang, Dezhu Huang, Jiajie Fan, *Senior Member, IEEE*, Fengman Liu, Tingyu Lin, Liqiang Cao, Xuejun Fan, *Fellow, IEEE*, Braham Ferreira, *Fellow, IEEE*, and Guoqi Zhang, *Fellow, IEEE*

**Abstract- In this paper, a microchannel thermal management system (MTMS) with the two-phase flow using the refrigerant R1234yf with low global warming potential is presented. The thermal test vehicles (TTVs) were made of either single or multiple thermal test chips embedded in the substrates, which were then attached to the MTMS. The system included two identical aluminum microchannel heat sinks (MHSs) connected in series in the cooling loop, which also consisted of a gas flowmeter, a miniature compressor, a condenser, a throttling device, and accessory measurement components. The experimental results showed that the thermal management system could dissipate a heat flux of 526 W/cm² while maintaining the junction temperature below 120 ºC. For SiC MOSFET with a higher junction temperature, e.g., 175 ºC, the current system is expected to dissipate a heat flux as high as about 750 W/cm². The effects of the rotational speed of the compressor, the opening of the throttling device, TTV layout on MHS, and a downstream heater on the cooling performance of the system were analyzed in detail. The study shows that the present thermal management with a two-phase flow system is promising cooling technology for the high heat flux SiC devices.**

## I. INTRODUCTION

The heat flux of the next-generation silicon insulated gate bipolar transistor (Si IGBT) used in pure and hybrid electric vehicles applications would be as high as 500 W/cm², more than three times of heat flux in comparison with the current level of 100-150 W/cm² [1]-[3]. As a promising wide bandgap device, silicon carbide metal-oxide-semiconductor field-effect transistor (SiC MOSFET) has many advantages such as higher

breakdown voltage, higher switching frequency, and lower switching loss [4]. As its form factor tends to be smaller, its heat flux can be even higher in comparison with Si IGBT with the same voltage blocking capability, even higher heat flux is anticipated [4]-[6].

Such high heat fluxes cannot be addressed by using conventional cooling solutions such as vapor chamber [7]-[8], and single-phase liquid cooling [9]-[12]. Vapor chamber in combination with forced convection could dissipate heat flux no more than 100 W/cm² [13], while single-phase liquid cooling could reach 350 W/cm² [14]-[16]. Recently, immersion pool boiling and liquid metal cooling schemes have been reported for high heat flux electronics [13], [18]-[20]. The immersion pool boiling, which requires dielectric fluid to be in contact with the ICs directly, is usually limited by the critical heat flux of dielectric fluid and thus has insufficient cooling capacity. The liquid metal has much better thermophysical properties using eutectic alloys of different materials such as gallium, indium, and tin [20], but it may not be compatible with the metal piping and fittings. The cost of liquid metal is also much higher in comparison with other coolants [21].

Two-phase flow boiling regimes have received extensive attention in power electronics applications in recent years. Taking advantage of the latent heat of liquid refrigerant during its boiling process, it can provide higher heat transfer coefficients, lower flow rates, more uniform surface temperatures, and lower pumping power than a single-phase cooling scheme [1], [22]-[24]. However, the refrigerant boiling requires a wise control of the pressure and temperature of the refrigerant in the evaporator, so that the flow boiling can be reached for isothermal heat absorption.

Much research effort has been devoted to the two-phase flow boiling in the microchannel thermal management system (MTMS) for electronics cooling [25]-[28]. R134a is a commonly used refrigerant. In our previous study, an experimental study of a compact two-phase cooling system using R134a as a refrigerant was performed for high heat flux electronic packages. The experimental results showed the evaporator system could dissipate over 380 W/cm² for the thermal test vehicle (TTV) while maintaining its temperature at about 90 ºC [28].

Although R134a is a chlorine-free and non-ozone-depleting hydrofluorocarbon refrigerant, it has relatively high global warming potential (GWP) of 1430, which are several orders of magnitude greater than $CO_2$, and has been banned in Europe for new mobile air conditioner [29]. According to the latest EU F-gas Regulation, all F-gases with GWP of more than 150 will be banned as the refrigerant or foam blowing agent in any hermetically sealed system from 2022 [30].

On the other hand, R1234yf has a GWP of only 4, which is much lower than R134a and has been adopted in Europe and is being proposed to replace R134a in some countries [30]-[32]. There are some reports on experimental studies of R1234yf as a drop-in replacement for R134a in an MTMS [29]-[32].

Nonetheless, there is little work reported on two-phase flow boiling heat transfer of R1234yf in a microchannel heat sink (MHS) for high heat-flux power electronics cooling.

In this paper, an MTMS with the two-phase flow for power electronics is presented. Si-based TTVs were designed and fabricated to evaluate the cooling performance of the proposed thermal management system. Environment-friendly refrigerant R1234yf with low boiling points was selected to fill to the system. The system mainly consisted of two identical aluminum MHSs, a miniature compressor, a condenser, a throttling device, and accessory measurement components. The cooling performance of the system with one single-chip TTV was first analyzed. Then, the effects of the rotational speed of the compressor, the opening of the throttling device, TTV layout on MHS, and a downstream heater on the cooling performance of the system were analyzed sequentially. Lastly, the performance potential of the thermal management system was also discussed.

## II. DESIGN OF THERMAL MANAGEMENT SYSTEM WITH TWO-PHASE FLOW

### A. MHS for SiC MOSFET Power Module

Fig. 1 shows the schematic of a SiC power module assembled on one MHS with flow boiling bubbles. Thermal interface material (TIM) is used between the power module and the MHS to reduce the contact resistance. The heat generated by SiC MOSFETs can be absorbed by taking full advantage of the latent heat of liquid R1234yf when it reaches boiling. Therefore, an MTMS is required to realize the phase-change and heat absorption in the MHS.
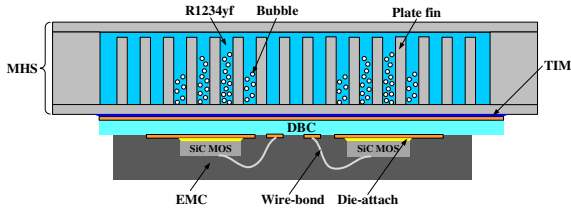


Fig. 1. Schematic of the SiC power module assembled on the MHS with two-phase flow boiling

### B. MTMS Design

Fig. 2(a) and (b) illustrates the experimental measurement platform and schematic diagram of the designed MTMS. The system mainly consists of MHS1 and MHS2 connected in series, a gas flowmeter, a miniature compressor, a condenser, a throttling device, and accessory measurement components. All the components were connected through copper tubes and fittings.

In the system, the compressor was used to increase the pressure of the refrigerant, while the throttling device was to reduce the pressure of the refrigerant and control the flow. The system was divided into a high-pressure (HP) region and a low-pressure (LP) region by the two components. The two MHSs and the gas flowmeter were in the LP region, and the condenser lay in the HP region.

The temperatures at the connection tubes of the LP region could be reduced to -10~-20 ℃ when the system was operating. To avoid the effect of heat loss on the cooling performance of the system due to the large temperature difference between the connection tubes and the ambient, the connection tubes in the LP region were protected with rubber foam tubes, as shown in Fig. 2(a).
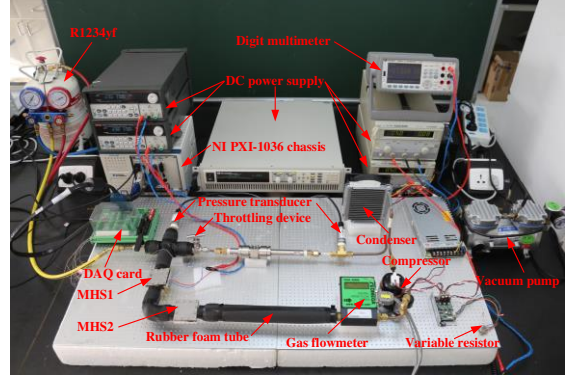


(a)
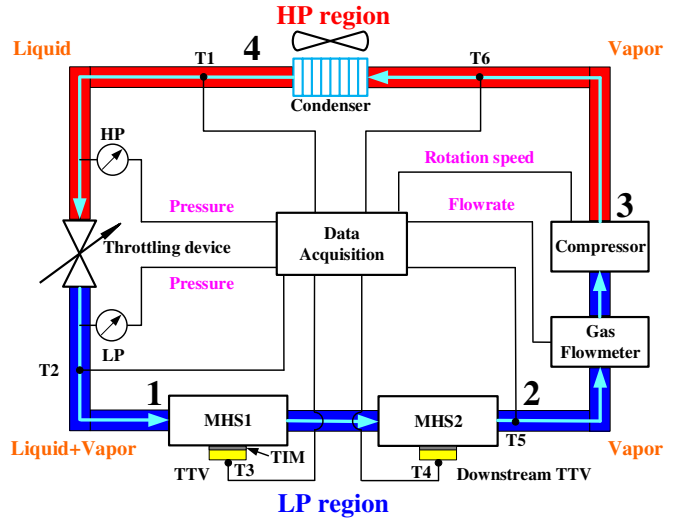


(b)

Fig. 2. MTMS: (a) Experimental measurement platform; (b) Schematic diagram

The MHS is a highly compact and lightweight aluminum plate fin evaporator. It has one inlet and one outlet tubes. The detailed size of MHS is shown in TABLE I. In the following III (A~D), MHS1 was used. In III (E), MHS1 and MHS2 were used.

TABLE I
THE SIZES OF MHS

| Part | Size (mm) |
| --- | --- |
| MHS | 50×50×9 |
| Base plate | 50×50×1 |
| Cover plate | 50×50×1 |
| Chamber | 30×30×7 |
| Plate fin | 20×0.5×6 |
| Channel spacing | 0.5 |
| Inner diameter of tube | 5.35 |
| Outer diameter of tube | 6.35 |

## C. TTVs Design

Currently, thermal test chip (TTC) using SiC is not available, to evaluate the cooling performance of the MTMS system, Si-based TTC from Thermal Engineering Associates Inc. was used to evaluate the cooling performance of MTMS. The size of a single TTC was $2.5 \times 2.5 \times 0.625$ mm³, which had two resistors in the same layer and four diodes in the other layer. The two resistors covered more than 85% of the chip area. The electric resistance of each resistor was 7.6 Ω ±10%.

Two TTVs based on substrate embedded packaging technology were designed and fabricated [28]. The detailed process of packaging of TTV1 with one chip and assembly on the MHS is shown in Fig. 3. A TTC was picked and placed in the center cavity of a substrate with the almost same thickness as the TTC, and temporarily bonded onto a carrier through a layer of temporary bond film (TBF). The two resistors of TTC in the TTV1 were connected in series and then bonded onto one edge of the substrate through gold wires. The total electric resistance of the TTV1 reached about 15.2 Ω. A thermocouple (TC) was directly attached to the top surface of TTC so that the junction temperature could be precisely monitored in real-time when it was operating. The TTC and TC were then encapsulated by ultraviolet (UV) adhesive to protect from damage. After that, the TTV1 was debonded from the carrier.
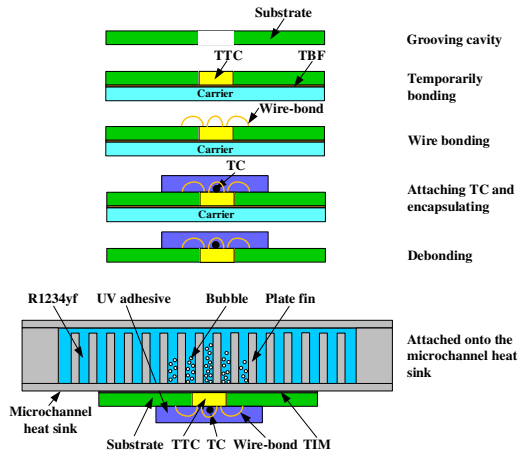


Fig. 3. Packaging of TTV1 and assembly process on MHS

For TTV2 with multi-chips, it used four TTCs in a 2×2 array without extra spacing. The eight resistors in the four TTCs were connected in series and then bonded to one edge of the substrate through gold wires. Compared with the TTV1, the effective area and the total electric resistance of the TTV2 increased by 4 times, which were 0.25 cm², and 60.8 Ω, respectively. The TTV1 and TTV2 samples are shown in Fig. 4(a) and (b), respectively.
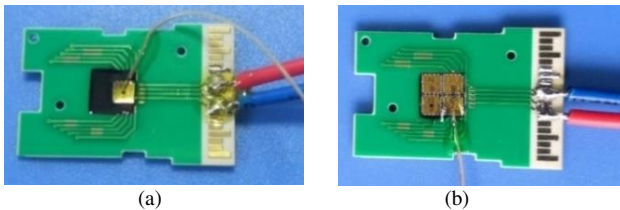


(a)                    (b)

Fig. 4. TTV samples: (a) TTV1; (b) TTV2

The TTV was directly attached to the bottom center of MHS through a layer of TIM. The TIM (TC-5888) from Dow Corning was used, which combined advantages of high thermal conductivity (5.2 W/m·K) and thin bond line thickness of approximately 20 μm, which yielded a low specific thermal resistance of 0.05 ℃·cm²/W.

## D. Other Components

A miniature rotary compressor (14-24-000X) from Aspen was used in the system, which is the smallest and lightest compressor available in the market as far as we know. Its suction volume was 1.4 cm³, and the maximum rotational speed was up to 6500 PRM, which can be adjusted by a variable resistor. The pressure and flow rate of refrigerant thus could be adjusted through the variable resistor.

A throttling device played a dual role in regulating the pressure drop across the throttling device and the flow rate and preventing large pressure drop oscillations across the test module.

For the condenser, an aluminum mini-channel heat exchanger was adopted, which was fabricated based on the mini-end milling process. To improve the convective heat transfer coefficient, a fan was applied to the condenser.

To accurately evaluate the cooling performance of the thermal management system, temperature, pressure, and other measurement components were connected to the system.

Six high precision Type K TCs (T1-T6) from OMEGA were to monitor the temperatures at different locations of the system. One of the attached locations is shown in Fig. 2(b). The positive and negative leads of the six TCs were connected to a high-resolution data acquisition device from National Instruments. We could read real-time temperatures via LabVIEW software. Before testing, the signals of TCs were calibrated and the reference temperature was set to 20 °C.

Two voltage output pressure transducers (PX309-200 G5V) from OMEGA were adopted to detect the pressures of the HP region and LP region, respectively. The absolute pressure range of the transducer was 0~14 bar, and the driver voltage/current was 5 V/0.1 A. The pressure changes in the evaporators were negligible compared to those in the throttling device and miniature compressor [34], so the two pressure transducers could provide the important data needed to assess the system performance. The pressures could be read in real-time in the form of voltages by a digit multimeter from KEYSIGHT. The calibration curve of the pressure $P_{PT}$ (bar) and the tested voltage $U_{PT}$ (V) is expressed in (1) [28].

$$P_{PT} = 2.32 \times U_{PT} + 0.565. \tag{1}$$

We could also indirectly acquire the rotational speed of the compressor via the digit multimeter. The voltage of the variable resistor $U_{VR}$ (V) could be read when the compressor was operating. The rotational speed of compressor $n$ (PRM) then can be calculated as follow.

$$n = \begin{cases} 0 & (4.3V \leq U_{VR} < 5V) \\ 7078.93 - 1157.89 U_{VR} & (0.5V \leq U_{VR} \leq 4.3V). \\ 6500 & (U_{VR} < 0.5V) \end{cases} \tag{2}$$

The gas flowmeter (FMA-4312) from OMEGA was used to monitor the vapor flowrate of refrigerant, which could be read in the electronic display. The driver voltage/current was 5 V/0.09 A. The flowrate range was 0~10 L/min.

The temperatures at different positions, the pressures of HP and LP regions, the flowrate of refrigerant, and the rotational speed of compressor could be recorded in real-time. Only were these parameters properly controlled, did the system have a better cooling performance.

*E.    Thermodynamic Analysis of R1234yf Refrigerant*

R1234yf from Honeywell was selected as the refrigerant and filled into the system. Fig. 5 shows the variation of pressure with the saturation temperature of R1234yf. The fit function is expressed as (3).

$$P_s=\exp\left(1.14119+0.03326T_s-9.33109\times10^{-5}T_s^2\right), \quad (3)$$

where $T_s$ is the saturation temperature of R1234yf, and $P_s$ is the corresponding pressure. As seen in the figure, the pressure of the refrigerant rises nearly quadratically with the saturation temperature. Under the same temperature, reducing the pressure can make the refrigerant change from liquid to vapor, and thus absorb a large amount of heat. Likewise, increasing the pressure can make the refrigerant change from vapor to liquid, and thus release a lot of heat.
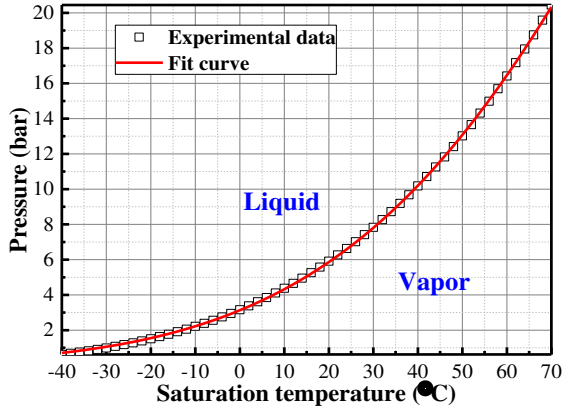


Fig. 5. Variation of pressure with saturation temperature of R1234yf

Fig. 6 shows a representative experimental working cycle of R1234yf in the system. An ideal pressure-enthalpy diagram of R1234yf was dotted in the figure, which was divided into the subcooled liquid, the liquid/vapor mixture, and the superheated vapor regions by a saturated liquid curve and a saturated vapor curve. The points 1~4 in the figure correspond to the system locations 1, 2, 3, and 4, shown in Figure 2.

As shown in Fig. 6, in the process 1-2, most of the heat generated by the TTV is absorbed by the liquid/vapor mixtures of R1234yf due to the vaporization of liquid refrigerant. The bubble grows and departs at a high frequency, forming bubbly flow and then slug flow in the microchannels between the plate fins of the MHS. The liquid/vapor mixtures fully change to the superheated vapor after heating. Then, the superheated vapor enters a gas flowmeter. Then, the superheated vapor goes to a compressor and is compressed to a higher pressure vapor, resulting in a higher temperature in the process 2-3. Next, the

compressed vapor R1234yf flows into a condenser, the superheated vapor changes to the subcooled liquid. The heat accumulated in the previous processes (1-3) is released to the ambient due to the latent heat of condensation of vapor refrigerant in the process 3-4. Lastly, the subcooled liquid refrigerant returns into the MHS1 through a throttling device, the subcooled liquid refrigerant changes into the liquid/vapor mixtures again, and the pressure drops drastically to a low level (process 4-1).
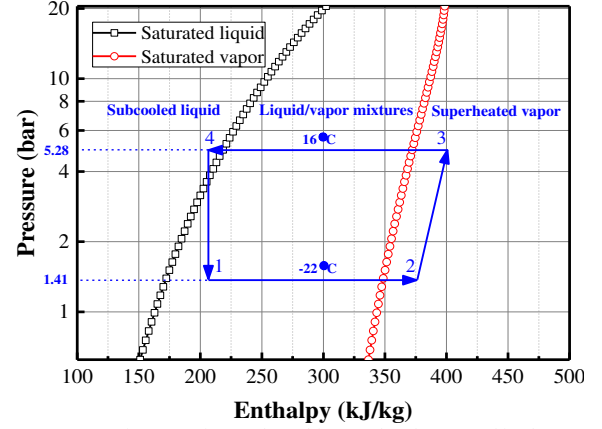


Fig. 6. Representative experimental working cycle of R1234yf in the system

## III. RESULTS AND DISCUSSION

*A.    Cooling Performance Evaluation with TTV1*

In this section, the cooling performance of the microchannel thermal management system was evaluated using TTV1. The measured electrical resistance of the TTV1 was 13.76 Ω through digit multimeter. A 200 V / 60 A DC power supply was adopted to drive the TTV1. The heat fluxes rising from 55 W/cm² to 526 W/cm² were tested by increasing the current from 0.5 A to 1.51 A.

Fig. 7 displays the junction temperature of TTV1 and the pressure of the LP region dependent on the heat flux of TTV1. As seen in the figure, the junction temperature of TTV1 increased almost linearly with the heat flux of TTV1. Particularly, when the heat flux of TTV1 increased from 55 W/cm² to 124 W/cm² (seen from insert), the junction temperature of TTV1 rose from 8 ℃ to 24.3 ℃, which was below the ambient temperature of 25 ℃. As shown in the figure, the pressure of the LP region remained about 1.8 bar. Combining (3) with Fig. 5, the saturation temperature of R1234yf at 1.8 bar was estimated to be -16 ℃. This means the junction temperature of TTV1 could be lower than the ambient temperature of 25 ℃ even when the heat flux of TTV1 reached 124 W/cm². On the other hand, when the heat flux of TTV1 increased to 526 W/cm², the junction temperature of TTV1 approached to 119 ℃, which was near the allowed highest junction temperature 125 ℃. For SiC devices with a higher junction temperature, e.g., 175 ℃ [33], the heat dissipation of the present system could go up to 750 W/cm² based on the same level of thermal resistance. Therefore, the thermal management system could dissipate a heat flux of 526 W/cm² while maintaining the junction temperature below 120 ℃.
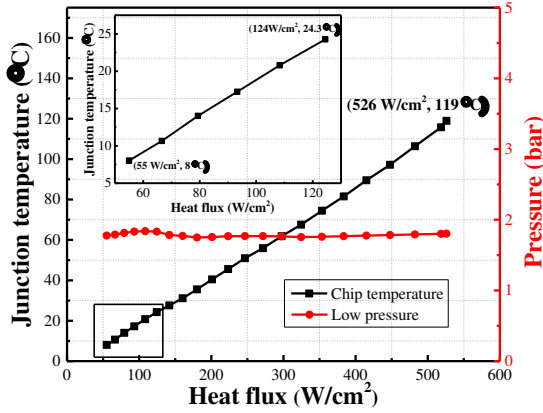
Fig. 7. Junction temperature of TTV1 and pressure of LP region dependent on heat flux of TTV1

### B. Effect of the Rotational Speed of the Compressor

In this section, the effect of the rotational speed of the compressor on the cooling performance of the system was analyzed under the same heat flux of TTV1. The rotational speed of the compressor was changed by adjusting the voltage of a variable resistor connected to the compressor controller. According to (2), when the voltage of the variable resistor decreased from 3.6 V to 3.2 V, the rotational speed increased from 2911 r/min to 3374 r/min.

Fig. 8 illustrates the junction temperature of TTV1 dependent on the rotational speed of the compressor under the heat flux of 229 W/cm$^2$. From the figure, it can be seen that the junction temperature of TTV1 first decreased and then increased with the rotational speed of the compressor. When the rotational speed of the compressor reached 3258 r/min, the junction temperature of TTV1 went down to 47.1 ºC, which lowered by 4.4 ºC compared with the rotational speed of 2911 r/min. During the system operation, the phase-change heat transfer of R1234yf depended on its flowrate and system pressure drop that could be controlled by adjusting the rotational speed of the compressor. Therefore, the rotational speed of the compressor could affect cooling performance of the system. Either too high or too slow flowrate would adversely affect cooling performance. In the following investigations, the rotational speed of the compressor was fixed to be 3258 r/min.
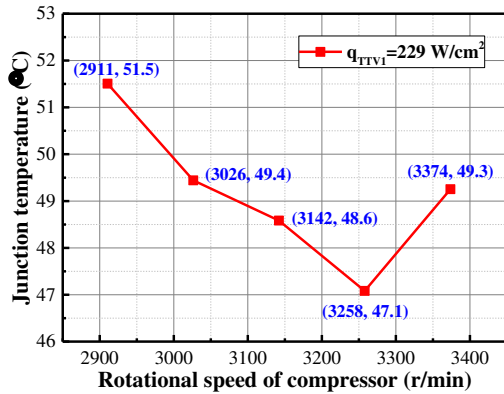


Fig. 8. Junction temperature of TTV1 dependent on rotational speed of compressor

### C. Effect of the Opening of the Throttling Device

In this section, the effects of changing the opening of the throttling device at the beginning and the testing process on the cooling performance were analyzed, respectively.

For changing the opening at the beginning, by applying the current from 0.5 A to 1.4 A, the heat flux of the TTV1 increased from 55 W/cm$^2$ to 449 W/cm$^2$ in the conditions of a small opening and a large opening, respectively. Fig. 9 shows the pressure drops across the throttling device and the junction temperatures dependent on the heat flux of TTV1 under both the small and large openings of the throttling device. As seen in the figure, the pressure drop across the throttling device was affected by the opening of the throttling device. A smaller opening led to a higher pressure drop. The pressure drops were about 4 bar and 3.1 bar under the small and large opening, respectively. Therefore, the opening of the throttling device can be quantified by its pressure drop.

As shown in Fig. 9, when the heat flux of the TTV1 increased from 55 W/cm$^2$ to 353 W/cm$^2$, the junction temperatures of the TTV1 under the pressure drop of 4 bar were lower than that under the pressure drop of 3.1 bar. When continuing increasing the heat flux of the TTV1, the junction temperature of the TTV1 under the pressure drop of 4 bar surpassed that under the pressure drop of 3.1 bar. Because only a small portion of refrigerants flew into the MHS1 under the pressure drop of 4 bar, complete phase-change of the fluid refrigerant could occur, the system showed better cooling performance at lower heat flux but deteriorated at high heat flux. This could be due to the lower flowrate in the MHS1, which could approach the dry-out limit at higher heat flux. As such, increasing the opening of the throttling device could increase the flowrate and reduce the junction temperature of the TTV1 at high heat flux, thus improving the cooling performance of the thermal management system.
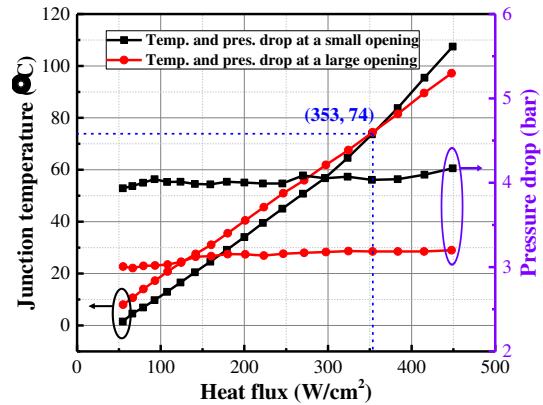


Fig. 9. Pressure drops across the throttling device and junction temperature dependent on heat flux of TTV1 under different openings of throttling device

For changing the opening at the testing process, by applying the current from 0.8 A to 1 A and then from 1 A to 1.1 A, the heat flux of TTV2 increased from 152 W/cm$^2$ to 244 W/cm$^2$ and then from 242 W/cm$^2$ to 297 W/cm$^2$. Fig. 10 shows the effect of the opening of the throttling device on the junction temperature of TTV2, the pressure drop across the throttling device. When the heat flux of TTV2 increased from 152 W/cm$^2$ to 244 W/cm$^2$, the junction temperature of TTV2 rose from 59.5

ºC to 107 ºC, and the pressure drop almost kept 2.92 bar. The refrigerant was approaching the dry-our regime due to the lower flow rate. At this moment, the opening of the throttling device was increased to observe its effect on cooling performance. The junction temperature and pressure drop significantly dropped, which decreased from 107 ºC, 2.92 bar to 92 ºC, 2.67 bar, respectively. Because new R1234yf flew into the MHS1 and more phase-change occurred, the cooling performance of the system was improved. Therefore, when the refrigerant is approaching the dry-out regime, the junction temperature of TTV2 can be reduced by increasing the opening of the throttling device at high heat flux, which allows more refrigerant into MHS and thus improves the cooling performance of the system without reaching the dry-out regime.
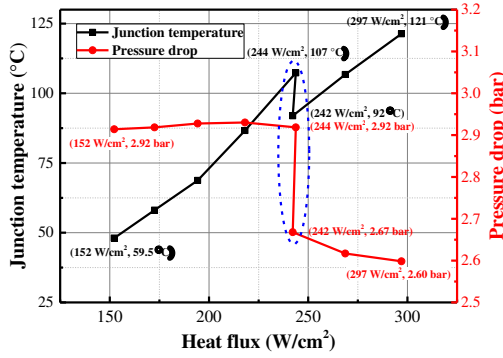


Fig. 10. Effect of opening of throttling device on junction temperature of TTV2 and pressure drop across the throttling device

### D. Effect of TTV Layout on MHS1

In this section, the junction temperature distributions of two TTV2 layouts on MHS1 were studied.

In the first layout, two TTV2s were arranged at the upstream and downstream along the centerline of MHS1, and their heat fluxes were both increased from 59 W/cm$^2$ to 202 W/cm$^2$. Fig. 11(a) shows the junction temperatures of the two TTV2s. As can be seen from the figure, when the heat flux of TTV2 reached 202 W/cm$^2$, the junction temperature of TTV2 at the upstream was 11 ºC lower than at the downstream. The heat generated by TTV2 was conducted through chip, TIM and MHS1 base to the chamber, making the liquid refrigerant between plate fins to vaporize. The phase-change could provide higher heat convection coefficients. The lower junction temperature of TTV2 at the upstream was due to the better cooling at the upstream with the fresh cold refrigerant, whereas the refrigerant was preheated to vaporize to some degree due to heat spreading effect, unfavorably affecting the cooling performance at the downstream.

In the second layout, two TTV2s were arranged at the lateral midstream, symmetrically to the centerline of the MHS1, and the heat fluxes were both increased from 59 W/cm$^2$ to 136 W/cm$^2$. Fig. 11(b) illustrates the junction temperatures of the two TTV2s, which were nearly the same. The junction temperature differential for the two lateral positions was only 3.3 ºC, even at the heat flux of 136 W/cm$^2$. However, compared with the cases arranged at the upstream and downstream, the heat dissipation capacity of the system with TTV2s arranged at the lateral midstream was greatly reduced, which was attributed

to the reduced flow distribution at the lateral channels instead of centerline channels. Therefore, for two TTVs with the same heat flux, it is suggested to allocate the TTVs at the two lateral positions; for multiple TTVs with different heat flux, it is recommended to put the TTVs at the centerline in the order of decreasing heat fluxes, with the highest one allocated at the upstream.



(a)



(b)

Fig. 11. Junction temperatures of two TTV2s layouts on MHS1: (a) Upstream and downstream; (b) Lateral midstream

### E. Effect of a Downstream TTV1 on MHS2

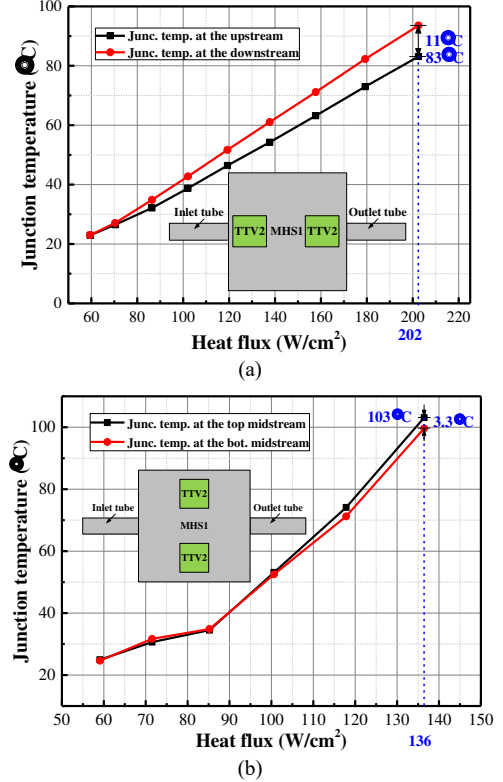In this section, MHS1 and MHS2 were used. A downstream TTV1 on MHS2 was introduced to study its effect on the pressure drop across the throttling device and junction temperature of the upstream TTV1 on MHS1. The downstream TTV1 could be viewed as either a regular heat-dissipating device or a super-heating device. The liquid R1234yf was expected to vaporize more completely in MHS2 upon absorbing heat from the downstream TTV1, thus increasing the enthalpy change of R1234yf before flowing into the condenser.

In the experiment, two 72 V / 1.2 A DC power supplies were used to drive the two TTV1s, respectively. By applying the current from 0.5 A to 1.15 A, the heat fluxes of both TTV1s were increased from 55 W/cm$^2$ to 297 W/cm$^2$.

Fig. 12(a) shows the pressure drops across the throttling device dependent on the heat flux of upstream TTV1 when a downstream TTV1 is used as a heat-dissipating device and a super-heating device, respectively. As seen from the figure, the pressure drop across the throttling device in the system with a downstream super-heating TTV1 was higher than that with a downstream heat-dissipating TTV1. The pressure differential increased slightly with the heat flux of the upstream TTV1. As discussed in Section III (C), a smaller opening of the throttling

device led to a higher pressure drop. Therefore, the downstream TTV1 could be a heat-dissipating device or super-heating device, which was determined by the pressure drop across the throttling device.

Fig. 12(b) shows the effect of a downstream TTV1 on the junction temperatures of TTV1s. Compared with the upstream TTV1 followed by a regular heat-dissipating TTV1, the junction temperature of the upstream TTV1 followed by a super-heating TTV1 dropped by 8 ℃ when their heat fluxes increased to 297 W/cm$^2$. Nonetheless, the junction temperature of the super-heating TTV1 increased evidently, which increased to 92 ℃. Because a few refrigerants flew into the MHSs under the high pressure-drop across the throttling device, the liquid R1234yf was vaporized more completely in MHS2 upon absorbing heat from the downstream TTV1, thus increasing the enthalpy change of R1234yf. Therefore, the upstream TTV1 followed by a super-heating TTV1 showed a lower junction temperature than that followed by a heat-dissipating TTV1. The refrigerant in the MHS2 was preheated to vaporize to some degree, unfavorably leading to the higher junction temperature of super-heating TTV1 than that of the heat-dissipating TTV1. The junction temperature of the heat-dissipating TTV1 was close to that of the upstream TTV1, but their temperatures were higher than that of the upstream TTV1 followed by a super-heating TTV1. Because enough refrigerant flew into the MHSs under the low pressure-drop across the throttling device, the phase-change rate was almost the same in the two MHSs. Therefore, the downstream TTV1 on MHS2 could function as a super-heating device while making the junction temperature of the upstream TTV1 on MHS1 at a lower value.
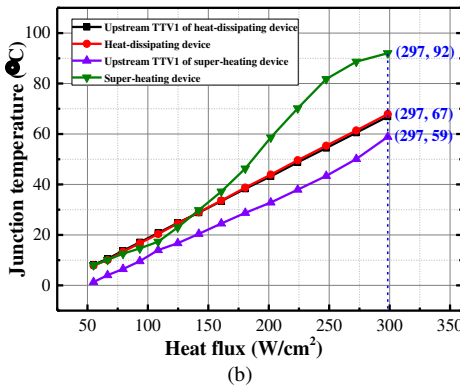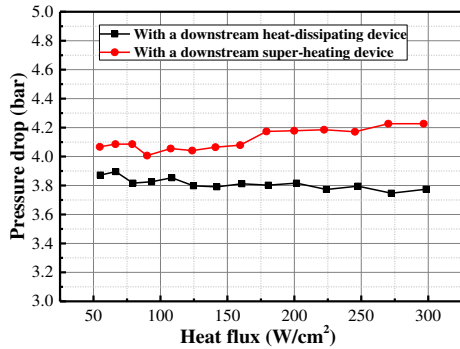




Fig. 12. Effect of a downstream TTV1 on MHS2: (a) Pressure drops across the throttling device; (b) Junction temperatures of TTV1s

*F. Discussion on Cooling Performance Enhancement*

In this study, various effect factors were studied to improve the cooling performance of the thermal management system. However, there is still some room to improve.

- A super-heating device can also be called as a sacrificed device, which can help to improve the cooling performance of the system. The maximum cooling performance of the system will be investigated under the sacrificed device.

- In this experiment, we found that the filling amount of R1234yf affected the cooling performance of the MTMS. Either over-filled or under-filled refrigerants would cause deterioration in cooling performance. A more detailed study on the filling amount will be conducted.

- Compared with the air-cooled condenser, a liquid-cooled condenser could improve the heat transfer capability from the system to the ambient. To achieve much better cooling performance, liquid-cooled condenser will be used in the future.

- In this experiment, a throttling device with a wide range of openings was used. However, only in the last turn, did the adjustment of the opening could affect the cooling performance. In the future study, a thermal expansion valve will be used to achieve precise control of the pressure drop. The maximum operating pressure of the thermal expansion valve should be slightly larger than the highest pressure of the present system. To study the effect of the opening of the throttling device on the cooling performance, an electrically controlled valve with program control will replace the throttling device in the present system.

- Further study on the affecting factors will be performed. Microchannel structures and inlet and outlet of the MHS will be optimized via computational fluid dynamics simulation. The effect of the mass flow rate of refrigerant on the cooling performance of the system will be studied.

- Single-sided MHS with two-phase flow boiling has been proved to be an effective cooling solution for high heat-flux TTV. If double-sided cooling is adopted, much more heat can be absorbed.

With the above-mentioned improvement techniques, the cooling performance of the system can be further improved to address the more demanding heat dissipation level, such as 1000 W/cm$^2$, which can be extended to the SiC MOSFETs power module.

## IV. CONCLUSION

In this paper, we developed a microchannel thermal management system with the two-phase flow. Single/multiple Si thermal test chips were packaged in the center cavity of a substrate. Thus, the thermal test chips in the thermal test vehicles (TTVs) could be directly attached to a microchannel heat sink (MHS) through a layer of TIM. To realize the two-phase flow in the system, low boiling-point R1234yf with environmental friendliness was selected to fill into the system. The system mainly consisted of two identical aluminum MHSs, a miniature compressor, a condenser, a throttling device, and temperature, pressure, and accessory measurement components. The cooling performance of the system with one single-chip

TTV1 was first analyzed. The experimental results showed the microchannel thermal management system can dissipate up to 526 W/cm$^2$ while maintaining the junction temperature of TTV1 below 120 ˚C. For SiC devices with a junction temperature, e.g., 175 ˚C, the current system is predicted to dissipate the heat flux as high as about 750 W/cm$^2$. Then, the effects of the rotational speed of the compressor, the opening of the throttling device, TTV layout on MHS1, and a downstream heater on MHS2 on the cooling performance of the system were analyzed sequentially. The study showed the opening of the throttling device had a great effect on cooling performance. For the multi-module system, the chip at the upstream had the best cooling performance. On the other hand, the downstream TTV on MHS2 could function as a super-heating device instead of a heat-dissipating device, making the junction temperature of upstream TTV at a low value.

## References

[1] P. Wang, P. McCluskey, Avram Bar-Cohen, "Two-Phase Liquid Cooling for Thermal Management of IGBT Power Electronic Module," *J. Electron. Packag.*, vol. 135, 021001-021001-11, Jun., 2013

[2] P. Wang, P. McCluskey and A. Bar-Cohen, "Hybrid Solid- and Liquid-Cooling Solution for Isothermalization of Insulated Gate Bipolar Transistor Power Electronic Devices," *IEEE Trans. Comp. Packg. Technol.*, vol. 3, no. 4, pp. 601-611, Apr. 2013.

[3] I. Aranzabal, I. M. de Alegría, N. Delmonte, P. Cova and I. Kortabarria, "Comparison of the Heat Transfer Capabilities of Conventional Single- and Two-Phase Cooling Systems for an Electric Vehicle IGBT Power Module," *IEEE Trans. Power Electron.*, vol. 34, no. 5, pp. 4185-4194, May, 2019.

[4] Shailesh N. Joshi, Ercan M. Dede, "Two-phase jet impingement cooling for high heat flux wide band-gap devices using multi-scale porous surfaces," *Appl. Therm. Eng.*, vol. 110, pp. 10–17, Jan. 2017.

[5] A. Bar-Cohen, J. D. Albrecht, and J. J. Maurer, "Near-junction thermal management for wide bandgap devices," in Proc. *IEEE Compound Semicond. Integr. Circuit Symp.*, Waikoloa, HI, USA, Nov. 2011, pp. 1–5.

[6] E. Laloya, Ó. Lucía, H. Sarnago and J. M. Burdío, "Heat Management in Power Converters: From State of the Art to Future Ultrahigh Efficiency Systems," *IEEE Trans. Power Electron.*, vol. 31, pp. 7896-7908, Nov. 2016.

[7] S. Wiriyasart, P. Naphon, "Fill ratio effects on vapor chamber thermal resistance with different configuration structures," *Int. J. Heat Mass Transf.* vol. 127, pp. 164–171, Dec. 2018.

[8] J. Zeng, S. W. Zhang, G. C., L. Lin, Y. L. Sun, L. Chuai, W. Yuan, "Experimental investigation on thermal performance of Al vapor chamber using micro-grooved wick with reentrant cavity array," *Appl. Therm. Eng.*, vol. 130, pp. 185-194, Feb. 2018.

[9] I. Mudawar, D. Bharathan, K. Kelly, and S. Narumanchi, "Two-Phase Spray Cooling of Hybrid Vehicle Electronics," *IEEE Trans. Comp. Packg. Technol.*, vol. 32, pp. 501-512, Jun. 2009.

[10] D. W. Yang, Y. Wang, G. F. Ding, Z. Y. Jin, J. H. Zhao, G. L. Wang, "Numerical and experimental analysis of cooling performance of single-phase array MHSs with different pin-fin configurations," *Appl. Therm. Eng.*, vol. 112, pp. 1547-1556, Feb. 2017.

[11] H. Y. Zhang, D. Pinjala, T. N. Wong, K. C. Toh, Y. K. Joshi, "Single-phase liquid cooled MHS for electronic packages," *Appl. Therm. Eng.*, vol. 25, pp. 1472-1487, Jul. 2005.

[12] H. Y. Zhang, D. Pinjala, Y. K. Joshi, T. N. Wong & K. C. Toh, "Development and Characterization of Thermal Enhancement Structures for Single-Phase Liquid Cooling in Microelectronics Systems," *Heat Transfer Engineering*, vol. 28, pp. 997-1007, Dec. 2007.

[13] N. Blet, S. Lips, V. Sartre, "Heats pipes for temperature homogenization: A literature review," *Appl. Therm. Eng.*, vol. 118, pp. 490-510, May 2017.

[14] Z. H. Wu, R. Du, "Design and experimental study of a miniature vapor compression refrigeration system for electronics cooling," *Appl. Therm. Eng.*, vol. 31, pp. 385-390, 2011.

[15] X. C. Tong, Advanced materials for thermal management of electronic packaging, Springer. New York, 2011.

[16] G. Tang, Y. Han, B. L. Lau, X. Zhang and D. M. W. Rhee, "Development of a Compact and Efficient Liquid Cooling System With Silicon Microcooler for High-Power Microelectronic Devices," *IEEE Trans. Comp. Packg. Technol.*, vol. 6, no. 5, pp. 729-739, May 2016.

[17] Y. Han, B. L. Lau, H. Zhang and X. Zhang, "Package-level Si-based micro-jet impingement cooling solution with multiple drainage micro-trenches," in proc. *2014 IEEE 16th Electronics Packaging Technology Conference (EPTC)*, Singapore, 2014, pp. 330-334.

[18] M. Tawk, Y. Avenas, A. Kedous-Lebouc and M. Petit, "Numerical and Experimental Investigations of the Thermal Management of Power Electronics With Liquid Metal Mini-Channel Coolers," *IEEE Trans Ind. Appl.*, vol. 49, no. 3, pp. 1421-1429, May-June 2013.

[19] M. Tawk, Y. Avenas, A. Kedous-Lebouc and M. Petit, "Study and realization of a high power density electronics device cooling loop using a liquid metal coolant", in proc *IEEE Energy Convers. Congr. Expo.*, Phoenix, AZ, 2011, pp. 36-43.

[20] M. Hodes, R. Zhang, L. S. Lam, R. Wilcoxon and N. Lower, "On the Potential of Galinstan-Based Minichannel and Minigap Cooling," *IEEE Trans. Comp. Packg. Technol.*, vol. 4, no. pp. 46-56, Jan. 2014.

[21] A. Heinzel, W. Hering, J. Konys, L. Marocco, K. Litfin, G. Müller, J. Pacio, C. Schroer, R. Stieglitz, L. Stoppel, A. Weisenburger, T. Wetzel, "Liquid Metals as Efficient High-Temperature Heat-Transport Fluids," *Energy Technol.* vol. 5, pp. 1026-1036, Feb. 2017,

[22] E.M. Fayyadh, M.M. Mahmoud, K. Sefiane, T.G. Karayiannis, "Flow boiling heat transfer of R134a in multi microchannels," *Int. J. Heat Mass Transf.*, vol. 110, pp. 422-436, Jul. 2017.

[23] T.G. Karayiannis, M.M. Mahmoud, "Flow boiling in microchannels: Fundamentals and applications," *Appl. Therm. Eng.*, vol. 115, 1372-1397, Mar. 2017.

[24] Mudawar I. "Two-Phase MHSs: Theory, Applications, and Limitations," *ASME. J. Electron. Packag.*, vol. 133, 041002-041002-31, Dec. 2011.

[25] C. Falsetti, M. Magnini, J. R. Thome, "Hydrodynamic and thermal analysis of a micro-pin fin evaporator for on-chip two-phase cooling of high density power micro-electronics," *Appl. Therm. Eng.*, vol. 130, 1425–1439, Feb. 2018.

[26] K. Liang, Z.H. Li, M. Chen, H.Y. Jiang, "Comparisons between heat pipe, thermoelectric system, and vapour compression refrigeration system for electronics cooling," *Appl. Therm. Eng.*, vol. 146, pp. 260-267, Jan. 2019.

[27] J. He, Y.T. Wu, X. Chen, Y.W. Lu, C.F. Ma, C.X. Du, G. Liu, R. Ma, "Experimental study of a miniature vapor compression refrigeration system with two heat sink evaporators connected in series or in parallel," *International Journal of Refrigeration*, vol. 49, pp. 28-35, Jan. 2015.

[28] F. Hou, W. Wang, H. Zhang, C. Chen, C. Chen, T. Lin, L. Cao, G.Q. Zhang, J.A. Ferreira, "Evaluation of A Compact Two-phase Cooling System for High Heat Flux Electronic Packages," *Appl. Therm. Eng.*, vol. 163, 114338, Dec. 2019.

[29] J. Navarro-Esbrí, J.M. Mendoza-Miranda, A. Mota-Babiloni, A. Barragán-Cervera, J.M. Belman-Flores, "Experimental analysis of R1234yf as a drop-in replacement for R134a in a vapor compression system," *International Journal of Refrigeration*, vol. 36, pp. 870-880, May 2013.

[30] Z.H. Li, K. Liang, H.Y. Jiang, "Experimental study of R1234yf as a drop-in replacement for R134a in an oil-free refrigeration system," *Appl. Therm. Eng.*, vo. 153, 646-654, May, 2019.

[31] J. Sieres, J. M. Santos, "Experimental analysis of R1234yf as a drop-in replacement for R134a in a small power refrigerating system," *International Journal of Refrigeration*, vol. 91, pp. 230-238, Jul. 2018

[32] A. Mota-Babiloni, J. Navarro-Esbrí, Á. Barragán, F. Molés, B. Peris, "Drop-in energy performance evaluation of R1234yf and R1234ze(E) in a vapor compression system as R134a replacements," *Appl. Therm. Eng.*, vol. 71, pp. 259-265, Oct. 2014.

[33] CREE. CPM2-1200-0025B, Rev. C. Accessed: Jan. 2016. [Online]. Available: https://www.wolfspeed.com/power/products/sic-mosfets/cpm2-1200-0025b.

[34] R. Mongia, K. Masahiro, E. DiStefano, J. Barry, W. Chen, M. Izenson, F. Possamai, A. Zimmermann, M. Mochizuki, "Small scale refrigeration system for electronics cooling within a notebook computer," in proc., *ITHERM*, San Diego, CA, 2006, pp. 751-758.